ELM burn-through predictions for MAST-U Super-X plasmas

S.F. Smith[1,2], S.J.P. Pamela[1], A. Fil[1], M. Hölzl[3], G.T.A. Huijsmans[4,5], A. Kirk[1], D. Moulton[1], O. Myatra[1,2], A.J. Thornton[1], H.R. Wilson[1,2]

[1] *CCFE, Culham Science Centre, Abingdon, UK.*

[2] *York Plasma Institute, Department of Physics, University of York, York, UK.*

[3] *Max-Planck-Institute for Plasmaphysics, EURATOM Association, Garching, Germany.*

[4] *CEA, IRFM, F-13108 Saint-Paul-lez-Durance, France.*

[5] *Eindhoven University of Technology, Eindhoven, The Netherlands.*

Edge localised modes (ELMs) are instabilities occurring in H-mode tokamak plasmas, resulting in filamentary structures that erupt violently from the plasma edge, degrading confinement and transporting heat and particles to the divertor. As a consequence, a high heat flux (HF) is incident on the targets, which will cause excessive erosion in future tokamaks [1]. One solution to address this focuses on divertor design; a new magnetic configuration called the "Super-X" is designed to alleviate high heat fluxes and will be tested on MAST-U [2]. Additional PF coils in the divertor region control the strike point radius position (R_s); at larger R_s the contact area of the plasma increases, thus reducing local heat fluxes. In addition, flux expansion in the chamber increases the neutral interaction volume and the divertor is designed to retain neutrals [3]; plasma detachment is predicted in the Super-X for L-mode [4] and H-mode [5] plasmas but behaviour during ELMy H-mode is unknown. Simulations to address this issue are presented here. The nonlinear MHD code JOREK [6] is used with a simple diffusive neutrals model [7], where the neutral density is

$$\frac{\partial \rho_n}{\partial t} = \nabla \cdot \left(\vec{D}_n : \nabla \rho_n\right) + S_{\rho_n} - (\rho \rho_n S_{ion} - \rho^2 \alpha_{rec}). \tag{1}$$

The diffusion coefficient ($\vec{D}_n$) is set to $2.1 \times 10^2\ m^2 s^{-1}$ in the following simulations and fits are made for the ionization (S_{ion}) and recombination (α_{rec}) rate coefficients [7]. A source term (S_{ρ_n}) is included allowing studies of injection and pumping. Separate equations are established for the ion and electron temperatures as follows

$$\rho \frac{\partial T_i}{\partial t} = -\rho\, \vec{v}_E \cdot \nabla T_i - \gamma p \nabla \cdot \vec{v}_E + \nabla \cdot (\kappa_{\perp i} \nabla_\perp T_i + \kappa_{\parallel i} \nabla_\parallel T_i) + \frac{1}{R^2} \eta j^2 + S_{T_i}, \tag{2}$$

$$\rho \frac{\partial T_e}{\partial t} = -\rho\, \vec{v}_E \cdot \nabla T_e - \gamma p \nabla \cdot \vec{v}_E + \nabla \cdot (\kappa_{\perp e} \nabla_\perp T_e + \kappa_{\parallel e} \nabla_\parallel T_e) + \frac{1}{R^2} \eta j^2 + S_{T_e} - \xi_{ion} \rho \rho_n S_{ion} - \rho \rho_n L_{lines} - \rho^2 L_{brem} \tag{3}$$

Here (ξ_{ion}) is the ionisation energy and line (L_{lines}) and Bremsstrahlung (L_{brem}) radiation rate coefficients are included. Reflective boundary conditions are implemented for the neutrals, as the plasma density is incident on the boundary it is reflected away as diffusive neutrals. This is described by the equation; $D_n \nabla \rho_n \cdot \vec{n} = -\xi_{ref} \rho \vec{v}_{\parallel} \cdot \vec{n}$, where the reflection coefficient (ξ_{ref}) is set to 95%. The MAST-U equilibrium is generated with an extended outer leg, using the Fiesta code [8] and is based on MAST H-mode pulse 24763 which is unstable to the peeling-ballooning modes that drive ELMs. The MHD parameters used in the simulations are as follows; $\eta = 5.3 \times 10^{-6}\ \Omega m$ (a factor 200 above the Spitzer value), $\mu_{\perp} = 2.7 \times 10^{-5}\ kgm^{-1}s^{-1}$, $\mu_{\parallel} = 2.7 \times 10^{-4}\ kgm^{-1}s^{-1}$. The hyper-resistivity and viscosity are included for numerical stability. Perpendicular particle and heat diffusivity profiles are used with a dip at the pedestal to represent the transport barrier. The parallel heat transport coefficients are $\kappa_{i\parallel} = 3.7\ kgm^{-1}s^{-1}$ and $\kappa_{e\parallel} = 1.5 \times 10^{2}\ kgm^{-1}s^{-1}$ (a factor 6.5 smaller than the Braginskii values). A scan in the upstream density has been established for the MAST-U Super-X case with expanded flux for JOREK, shown in Fig. 1 a). In JOREK, a roll-over in the target density flux is seen as the upstream density is increased, as well as a reduction in the electron temperature at the target to a few eV. It is also possible to see the ionisation front, in the lower divertor, move upstream as the upstream density is increased Fig. 1 b), indicating a high neutral density, cold divertor, which can be used for ELM burn-through simulations. This case has been compared to a SOLPS simulation [5] to evaluate the diffusive neutrals model. The differences between JOREK and SOLPS in $\Gamma_{e,targ}$, after the roll-over, could be due to the physics which missing in JOREK such as charge exchange, the inclusion of deuterium molecules and carbon impurities. ELM simulations are performed using a case without expanded flux, where a roll-over has also been established. Starting after the roll-over with a cold divertor, a single mode number perturbation of n=20 is introduced. Fig. 2 a)-h) shows the evolution of the simulation. After a cold divertor is obtained Fig. 2 a) & b), an ELM crash in the nonlinear phase occurs Fig. 2 c) & d), where filaments are formed and move

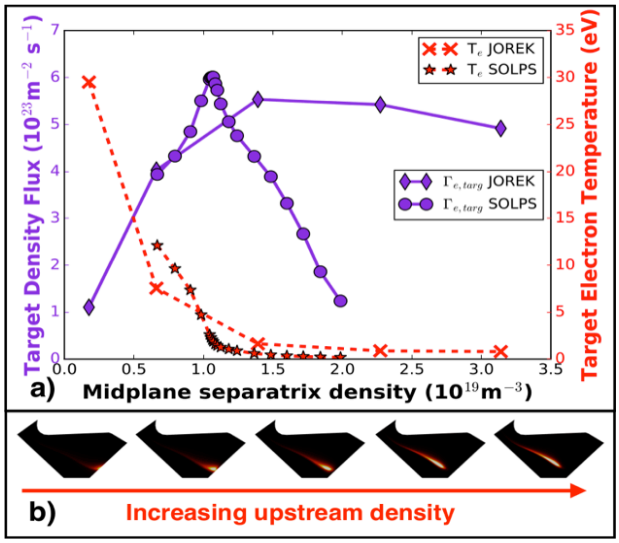

Fig. 1 a) Target density flux and electron temperature as a function of upstream density, comparison of JOREK to SOLPS. b) Ionisation in the lower divertor chamber as a function of upstream density, corresponding to each upstream density point in a).

out into the SOL. The heat and particles are transported to the divertor and the plasma burns through the neutrals front, as the neutrals become ionised. Around 0.2 *ms* after the start of the crash the peak HF is incident on the outer target of the Super-X, Fig. 2 e) & f). However, due to the large increase of plasma onto the targets an increase in neutral density is seen Fig. 2 h) and around 1-2 *ms* after the crash, the pre-ELM HF and electron temperatures are recovered Fig. 2 g) & h). A scan in reflectivity is given in Fig. 3, it shows that at higher reflectivity the divertor state can be recovered after an ELM crash. With 95% reflectivity, the HF and electron temperature onto the targets has recovered to almost pre-ELM conditions ~1-2 *ms* after the ELM crash. From Fig. 3) when the reflective coefficient is reduced (less neutrals in the divertor) there is no recovery observed in the electron temperature. Oscillations in the peak target values are seen in Fig. 3, these are related to the filaments arriving at the target, which then causes an increase in reflected neutrals. Multi-mode number simulations were performed (n=2,4,…,20), limited by computational resources, to attempt to produce a more realistic ELM crash; here the violent crash results in more suppressed MHD activity after the ELM in comparison to a single mode number simulation, where the filamentary oscillations are long-lived. As the ELM crash occurs the n=10 mode number is dominant; this was true for a single mode number simulation where higher toroidal mode number growth rates became suppressed. The evolution of the peak outer target values are shown in Fig. 4 a). It is seen that the peak HF to the outer target of the Super-X is 9.5 MW/m^2, which is an order of magnitude more than the single n=20 mode number simulation; the peak HF arrives to the target ~ 0.1 *ms* after the ELM crash and recovers ~1.5 *ms* after the crash. The peak HF to the baffle is 2.0 MW/m^2. Fig. 4 b)-d) shows the density, electron temperature and

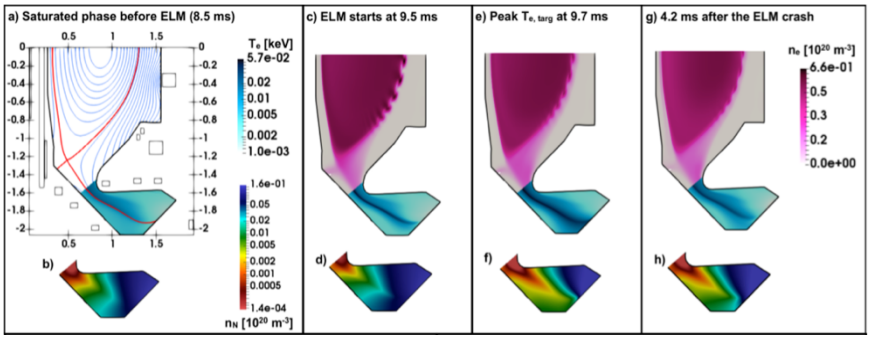

Fig. 2 Poloidal a) flux contours (blue), separatrix (red), divertor temperature and b) divertor neutral density. Plasma density and temperature c) and divertor neutral density d) at the start of the ELM. Plasma density and temperature e) and neutral density f) 0.2 *ms* after. Plasma density and temperature g) and neutral density h) at 4.2 *ms* after crash. Note: the lower half of MAST-U is shown but a full tokamak grid is used in the simulations.

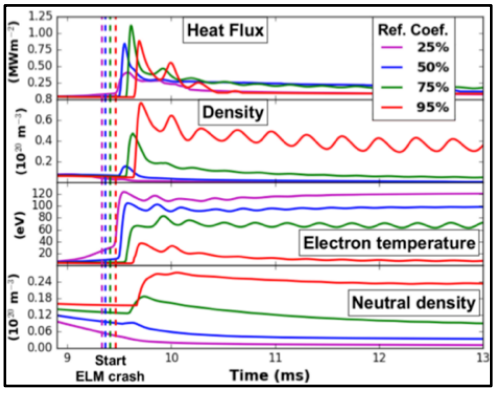

Fig. 3 Evolution of the peak outer target HF, density, electron temperature and neutral density for a reflectivity scan.

the connection length in the poloidal plane during the ELM crash. The density filaments, in Fig. 4 b), are seen to extend further into the SOL and finger-like structures are observed around the X-point and in the divertor region, seen also in the electron temperature, Fig. 4 c). Investigating the magnetic field structure (Poincaré plot Fig. 4 d)) it can be seen to roughly follow the temperature and density surfaces.

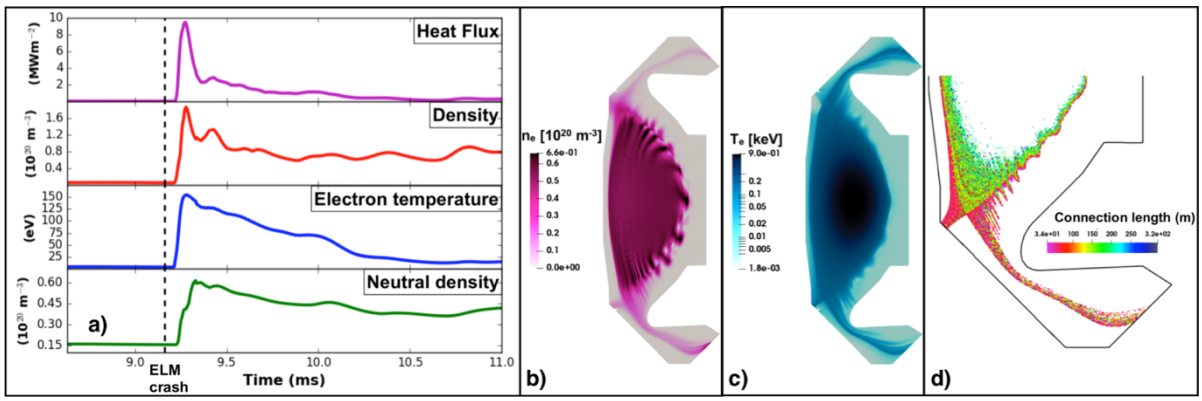

Fig. 4 a) Evolution of the peak values to the outer target. Poloidal plot of plasma density b) and electron temperature c) during the ELM. d) Poincaré plot of magnetic field structure during the ELM.

The first results with the diffusive neutrals model show the plasma burning through the neutrals front and re-attaching during an ELM. Reduced HF to the outer target is observed but the HF to the baffle, due to its position, could be a problem during large ELMs. Recovery times are on the order of the inter-ELM phase, however, if a pump was included in the simulation it is expected the recovery time would increase; and so, a pumping scan is under way to investigate neutral pumping in the divertor during an ELM crash. In the simulation phase before the ELM there appears to be a pumping threshold at which the plasma re-attaches. To obtain more realistic observations, additional physics in the model could be investigated.

Acknowledgements
This work has been carried out within the framework of the EUROfusion Consortium and has received funding from the Euratom research and training programme 2014-2018 and 2019-2020 under grant agreement No 633053 and from the RCUK Energy Programme [grant number EP/P012450/1]. To obtain further information on the data and models underlying this paper please contact PublicationsManager@ukaea.uk*. The views and opinions expressed herein do not necessarily reflect those of the European Commission. Funding from the EPSRC Fusion CDT grant number EP/L01663X/1, is acknowledged.

References

[1] R. Pitts et al., J. Nucl. Mater. **438**, S48 (2013)

[2] W. Morris et al., IEEE Transactions on Plasma Science **46**, 1217 (2018)

[3] I. Katramados et al., Fusion Eng. Des. **86**, 1595 (2011)

[4] E. Havlíčková et al., Plasma Phys. Controlled Fusion **57**, 115001 (2015)

[5] D. Moulton et al., O5.129, 44th EPS Conference, Belfast, Northern Ireland (UK), Tech. rep.

[6] G. Huysmans and O. Czarny, Nucl. Fusion **47**, 659 (2007)

[7] A. Fil et al., Physics of Plasmas **22**, 062509 (2015)

[8] L. Pangione et al., Fusion Eng. Des. **88**, 1087 (2013)